Korean J. Chem. Eng., **30**(10), 1855-1866 (2013)
DOI: 10.1007/s11814-013-0125-5

Characterization of TiO_2-coated ceramic foam prepared by modified sol-gel method and optimization of synthesis parameters in photodegradation of Acid Red 73

Somayeh Alijani, Abdolsamad Zarringhalam Moghaddam†, Mohammad Vaez, and Jafar Towfighi

Department of Chemical Engineering, Tarbiat Modares University, Jalal Ale Ahmad Highway, P. O. Box 14155-143, Tehran, Iran
(*Received 9 December 2012 • accepted 10 July 2013*)

Abstract−TiO_2 nanoparticles were synthesized by the P-25 powder modified sol-gel method under different TTIP (Titanium tetraisopropoxide) concentrations, P-25 loading and the gelation pHs. Structural properties of nanoparticles were characterized by XRD, FESEM and BET analysis. Results show that crystallinity level, particle size and the surface area are a function of P-25 loading and gelation pH, whereas TTIP concentration affects only the crystalline composition. Response surface methodology based on central composite design was used to optimize these synthesis parameters in photodegradation of Acid Red 73. The degradation efficiency was significantly affected by P-25 loading, pH value of gelation and the interaction effect between TTIP concentration and P-25 loading. The optimal values of parameters were found to be a pH of 1.34, a TTIP concentration of 0.25 M and a P-25 loading of 39.76 g/L. At optimal synthesis conditions, TiO_2 film was coated on alumina foam and its structural properties were characterized by XRD, SEM and BET technique. The photocatalytic activity of the as-prepared films was found to be higher than that of the films prepared by the sol-gel method and those made from the slurries of P-25. The reasonable photocatalytic performance and good stability offered by the optimized film make it as an effective alternative for large application of water treatment.

Key words: Titanium Dioxide, Modified Sol-gel Method, Structural Properties, Response Surface Methodology, Immobilization on Alumina Foam

INTRODUCTION

Among the photocatalytic processes catalyzed by oxide semiconductors, TiO_2 is the most commonly used semiconductor photocatalyst due to its high effectivity and stability with low toxicity and adequate price [1-4]. However, much research has been performed on the slurry system with the suspension of fine powdered TiO_2. The main problem of these systems is the post-treatment removal of TiO_2 powder, which can be time consuming and uneconomical. Therefore, the development of supported TiO_2 nanoparticles has been attractive to promote the feasibility of using the heterogeneous photocatalytic technology for water treatment [5]. A variety of materials have been explored as TiO_2 support in the photocatalytic processes to enhance surface contact with contaminants and improve the process economics [6]. Very few studies have been devoted to using macroporous inorganic materials as substrate [7]. Recently, the photocatalytic activity of immobilized TiO_2 particles on macroporous ceramic alumina foams has been reported [7-9]. Authors have concluded that reticulated macroporous ceramic foam supported TiO_2 with a three-dimensional and tortuous pore structure improving the light penetration and fluid flow is highly promising support for photocatalytic applications and water purification systems [8,9]. As reported by these studies, the method used for preparation of films on macroporous alumina foam is dip coating from suspension containing commercial titania nanopowders. Ochuma et al. [9] coated the alumina reticulated foam with a suspension of Degussa P-25 TiO_2 and compared its photocatalytic efficiency with suspended TiO_2 during DBU degradation. Plesch et al. [7] prepared TiO_2-coated alumina foam using Degussa P-25 as a TiO_2 nanopowder source and studied the effect of the porosity of the as-prepared catalyst on the photocatalytic activity in mineralization of phenol. However, as suggested by the literature, employing self-made powder can lead to films with sufficient mechanical stability and good adhesion, and they can be easily doped with various dopants to improve their photocatalytic activity [10,11]. The synthesis of self-made powders by the sol-gel method has been reported as the most frequently used technique for the preparation of TiO_2-based photocatalysts [12]. Vargová et al. have recently prepared TiO_2 film on reticulated alumina foam using titania precipitated by sol-gel technique [8]. They found that the TiO_2 films synthesized by sol-gel deposition method exhibited lower photocatalytic activity compared to layers made of suspension, and this limits the use of the derived sol-gel coatings on alumina foam in water purification applications. Regarding the benefits derived from preparing TiO_2 by sol-gel method, which include the production of homogeneous films with controlled morphology, high purity and durability, the improvement of photocatalytic performance of the derived sol-gel films on alumina foam has provided the impetus for the current research.

Many investigators have tried to improve the morphology of the derived sol-gel TiO_2 film by employing different experimental conditions [12-16]. Some studies have reported that incorporation of commercial TiO_2 powder into the sol-gel precursor solution (i.e., defined as a P-25 powder-modified sol-gel method) can result in

†To whom correspondence should be addressed.
E-mail: zarrin@modares.ac.ir

thicker films with improved photocatalytic activity, excellent adhesion and hardness with respect to those obtained by means of the unmodified sol-gel method [14,16-20]. Therefore, for the first time, we immobilized TiO_2 film onto alumina foam via P-25 powder-modified sol-gel method to improve the structural properties and photocatalytic performance of TiO_2 film immobilized on alumina foam.

In addition to Degussa P-25 loading, the structure and photocatalytic performance of TiO_2 synthesized by P-25 powder modified sol-gel method can be affected by other synthesis parameters such as pH gelation, concentration of titania precursor, calcination temperature, and impurities.

Therefore, in present study, first, TiO_2 nanoparticles were prepared by P-25 powder-modified sol-gel method (PPMSG), and the effect of synthesis parameters on the structural properties and photocatalytic efficiency of TiO_2 catalysis was studied. This is the first report on investigation of the effects of P-25 loading, titanium precursor concentration and different pH values of gelation on the structural properties and photocatalytic activity of TiO_2 nanoparticles prepared by PPMSG method during the degradation of Acid Red 73.

To study the interactions among the investigated parameters, in another stage, central composite design (CCD) based on the response surface methodology (RSM) was employed to study the interaction effect of selected factors on the photocatalytic degradation of Acid Red 73 using the TiO_2 catalysts formed from PPMSG procedure. The optimum value of these parameters was determined from the model obtained via the experimental design and analysis.

Finally, based on the optimum condition obtained from the experimental design, the titania nanoparticles were immobilized on reticulated alumina foam using sol precipitated by PPMSG method and photocatalytic activity was compared with the derived sol-gel TiO_2 films and those prepared using slurries of P-25 nanopowders.

EXPERIMENTAL

1. Reagents

Commercial ultrapure titanium tetraisopropoxide (purity 98%, TTIP, $Ti(O\text{-}i\text{-}C_3H_7)_4$), ethanol (98%, EtOH) with absolute grade and nanophase AEROXIDE TiO_2 P-25 powder (50 m^2/g; the ratio anatase-to-rutile of 80 : 20; the mean particles diameter of 21 nm) were used without any further purifications. Acid Red 73 ($C_{22}H_{14}N_4Na_2O_7S_2$, Mw=556.48 g/mol) purchased from the Ciba Company was applied as a model acid dye. All the chemicals were of analytical grade and supplied by Merck.

2. Synthesis of TiO_2 Nanoparticles

TiO_2 nanocrystals were prepared by the P-25 powder-modified sol-gel method (PPMSG) method as follows: various volume of titanium isopropoxide was dissolved in a 20 mL of anhydrous ethanol to provide solution with various TTIP concentrations (Table 1). The solution was stirred at room temperature for 30 min. Then, a certain volume of mixture containing deionized water and dilute nitric acid was added dropwise (1 mL/min) to the above solution during vigorous stirring to adjust the pH solution to a desirable value (Table 1). The acid was used as hydrolysis catalyst. After stirring for 1 h, P-25 powder with a loading according to Table 1 was used to prepare TiO_2-powder modified sol. Commercial TiO_2 powder was ultrasonically dispersed in the sol to minimize the formation of large agglomerates. The obtained white dispersion was then aged for 12 h followed by gelation at room temperature. The resultant gel was dried at 80 °C for 10 min and then calcinated at 600 °C for 1 h with a heating and cooling rate of 1 °C/min. The unmodified sol (i.e., plain sol) was also prepared by the similar procedure with the exception of adding TiO_2 P-25 powder.

Table 1. Experimental range and levels of the independent test variables

Variables	Ranges and levels				
	−2	−1	0	+1	+2
TTIP concentration (M) (x_1)	0.1	0.18	0.3	0.42	0.5
P-25 loading (g/L) (x_2)	10	18.10	30	41.89	50
Gelation pH (x_3)	1	1.2	1.5	1.8	2

3. Characterization

To investigate the effects of P-25 loading, pH gelation and the precursor concentration individually, the structural and morphological properties of TiO_2 powder prepared by PPMSG method were characterized. The XRD patterns of the prepared titania nanoparticles were obtained by using a PHILIPS PW1800 analyzer with a Cu Ka X-ray source. The rutile content in samples can be calculated by the following equation [21]:

$$X_R = \frac{(I_R/I_A)0.79}{1+(I_R/I_A)0.79}$$

where X_R is the mass fraction of the rutile phase in the sample, and I_A and I_R are the integrated X-ray intensities of the (1 0 1) reflection of anatase at 2θ=25.4° and the (1 1 0) reflection of rutile at 2θ= 27.5°, respectively.

The main grain size (L) can also be determined according to Scherrer's formula [22]:

$$L = \frac{0.89\lambda}{\beta\cos\theta}$$

where λ is the X-ray wavelength, β the full width at the half-maximum of the diffraction peak (FWHM) and θ the diffraction angle.

Field emission scanning electron microscopy (FESEM) was used (Hitachi S-4160) to determine the morphology of the powders. The specific surface area of samples synthesized by PPMSG method was measured by nitrogen adsorption-desorption at 77 K using the Brunauer-Emmett-Teller (BET) method with a Micromeritics 2000 instrument (ASAP 2000, Micromeritics, USA).

4. Experimental Design and Optimization by Response Surface Methodology

Response surface methodology (RSM), as an effective and reliable method in the experimental design, takes into account the interaction effects between a group of experimental parameters and presents their relation with the observed results by deriving a model [23]. Besides the simplifying the process by recognition of the most influential factors, RSM determines accurately a level combination of the studied variables which optimize the process. The application and development of RSM in photocatalytic process has attracted a wide range of interest due to its ability in reaching the optimal degradation efficiency with demand of less time, money and reagents [24,25].

In this study, we investigated the experimental conditions in the preparation of nanosized TiO_2 powders by P-25 powder-modified sol-gel method and optimized in the photodegradation of Acid Red 73 using response surface methodology. The Design Expert 7.0 software was used to analyze the experimental findings obtained under changing synthesis conditions. Three independent variables chosen in this work were the concentration of titania precursor (TTIP concentration), P-25 loading and gelation pH, with the degradation percentage of Acid Red 73 as the dependent variable (response). The ranges and levels of the studied variables are given in Table 1.

Central composite design (CCD) at five levels, as the most popular form used of RSM, was applied to evaluate the simultaneous effect of TTIP concentration, P-25 loading and gelation pH on the photocatalytic degradation of Acid Red 73 in 20 sets of experiments. All 20 experimental runs for estimation of the response variable were conducted in accordance with Table 1 of the supplementary materials. The experimental results of CCD were fitted with a second-order polynomial model by a multiple regression technique as follows:

$$Y(\%)=b_0+b_1x_1+b_2x_2+b_3x_3+b_{12}x_1x_2+b_{13}x_1x_3+b_{23}x_2x_3+b_{11}x_1^2+b_{22}x_2^2+b_{33}x_3^2$$

where Y stands for the response variable (degradation efficiency), b_i, b_{ii} and b_{ij} represent the regression coefficients of linear and quadratic effects and the interaction coefficients of parameters, respectively, and x_i's indicate the independent variables. The basic concepts in RSM and more details have been explained elsewhere [24,26,27].

5. Photocatalytic Activity Measurement

A series of photocatalytic experiments, called runs, was carried out using TiO_2 nanoparticles (0.1 g/L) synthesized by PPMSG method, and the obtained results were used for experimental design and optimization of the system. The photocatalytic activities of TiO_2 powders were assessed by the photodegradation of Acid Red 73 as the model compound. Experiments were performed in a batch-mode rectangular reactor made of Pyrex glass with total volume of 1 L. Four UV-A lamps (9W, Philips), positioned parallel to each other in the box, provided the artificial irradiation. The scheme of the employed photocatalytic reactor has been presented in our previous work [28]. The irradiation intensity of lamps measured by a UV radiometer (UVA 365 Lutron) was approximately 1.8 mW/cm^2. The dye solution was bubbled using two air pumps with a 1 L/min flow rate. The reactor was cooled by a fan placed at the box. Before each experiment, the aqueous solution of acid dye was agitated with gentle air in the presence of TiO_2 sample in the darkness for at least 30 min to achieve the complete equilibrium of adsorption process. Photocatalytic degradation processes were performed at 298 K with 250 mL of solution and an initial Acid Red 73 concentration of 20 mg/L. At certain time intervals, samples were taken out and then analyzed by an Optizen 3220UV double beam spectrophotometer. Before the measurement of residual dye concentration, each sample was filtered (pore size <0.22 μm) to remove any possible TiO_2 particles present in the solution. The maximum wavelength (λ_{max}) of Acid Red 73 is 545 nm. All of the experiments were carried out at fixed radiation time of 60 min.

6. TiO_2 Film Coating on the Alumina Foams

To obtain coated samples, 10 PPI (10 pores per inch) reticulated macroporous alumina foams of the dimension 95 mm×45 mm and a thickness of 10 mm purchased from M.S.A company were used as substrate. The titania coating was carried out by dipping the alumina foam into the TiO_2-powder modified sol for 10 min, followed by a drying procedure at 80 °C for 10 min. It is pointed out that the sol was prepared under optimized synthesis conditions derived by response surface methodology. The coating process was performed three-times. Subsequently, the coated samples were calcinated at 600 °C for 1 h with a heating and cooling rate of 1 °C/min. For comparison, a similar coating process was also followed using slurries of P-25 nanopowder and titania precipitated by unmodified sol-gel. It is noted that the loading of P-25 in the slurry was the optimal value obtained from optimization module in Design-Expert.

X-ray diffraction (XRD) measurements of the coated samples involved using the analyzer applied for the characterization of TiO_2 powders (PHILIPS PW1800, λ=0.1506). Scanning electron microscopy (SEM) (EM 3200) images of the coated samples were obtained after Au coating by a sputtering method. The specific surface area of samples was determined by the BET method, in which the N_2 adsorption at 77 K using the device utilized for the measurement of specific surface area of TiO_2 nanoparticles (ASAP 2000, Micromeritics, USA).

The photocatalytic activity of the titanium dioxide-coated alumina foams was also evaluated in the terms of photodegradation of Acid Red 73 in the same photoreactor as employed for the assessment of photoactivity of plain TiO_2. The equipment and method were the same as described in Section 2.5. The photocatalytic degradation processes were performed at 298 K using a solution containing 250 mL of a 20 mg/L Acid Red 73. An Optizen 3220UV double beam spectrophotometer was used to measure the residual dye concentration in the samples taken out at certain time intervals.

RESULTS AND DISCUSSION

1. Effect of Precursor Concentration

Table 2 and Fig. 1(a) exhibit the structural properties of the samples prepared with different concentration of precursor. We can see that TTIP concentration induces the variation of anatase to rutile ratio. The samples synthesized at low and high concentrations of TTIP become crystalline with predominantly anatase phase. However, for the middle concentrations, the samples contain both anatase and rutile phase together, which can affect the photocatalytic performance. As seen in Table 2 and Fig. 1(a), no significant changes in crystallinity degree and surface area can be noted for the powders prepared with different TTIP concentration.

2. Effect of P-25 Loading

Fig. 1 of the supplementary materials shows the X-ray diffractograms for samples prepared with different P-25 loading in the modi-

Table 2. Physical properties of TiO_2 powders obtained from modified sol-gel method at different TTIP concentration, gelation pH: 1.5 and P-25 loading: 30 g/L

TTIP concentration (M)	Crystal size (nm)	Anatase content (%)	S_{BET} (m^2/g)
0.1	35.75	95	21.36
0.3	42.29	75	22.58
0.5	39.84	89	23.29

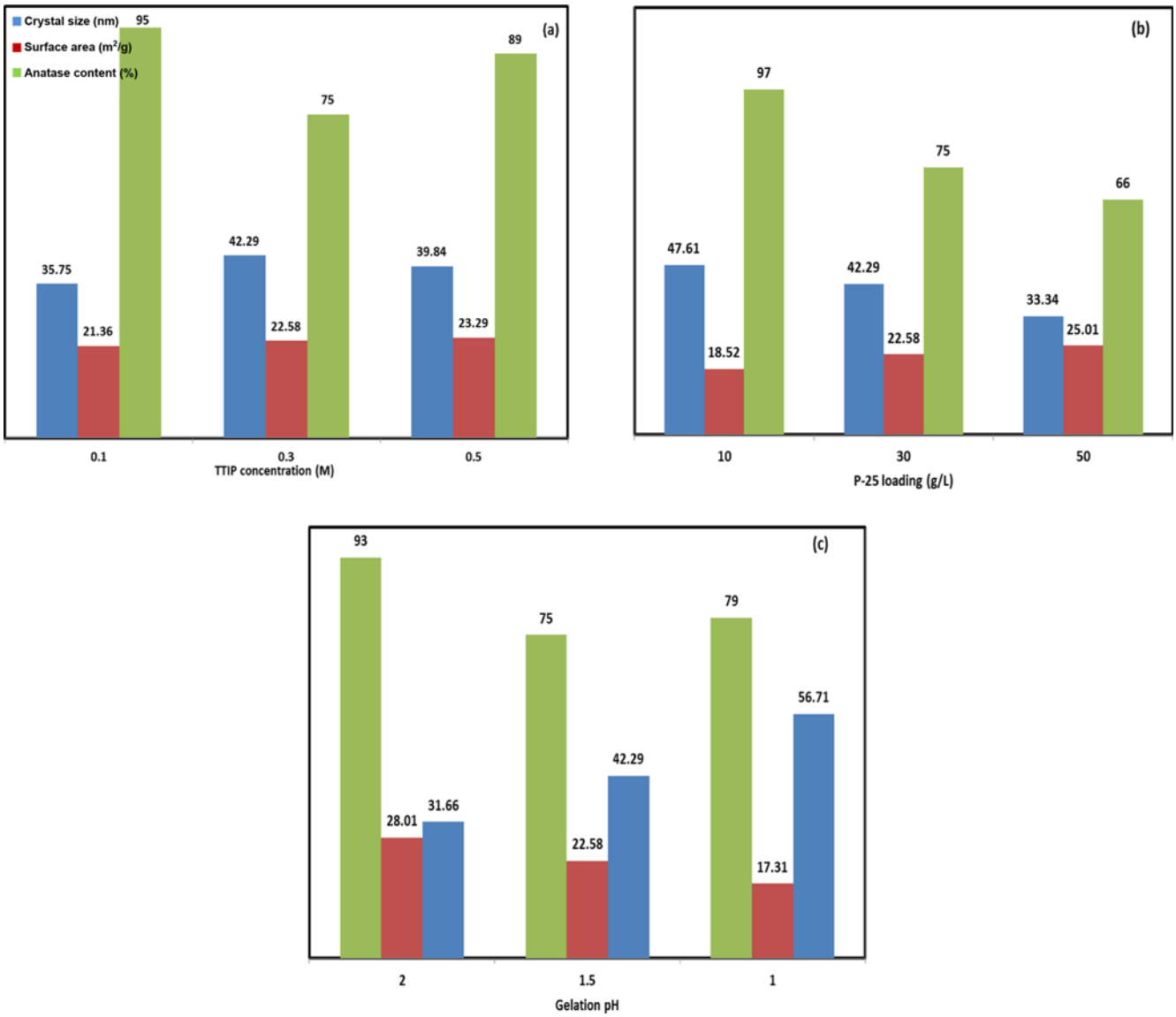

Fig. 1. Effect of synthesis parameters on the physical properties of TiO_2 nanoparticles prepared by P-25 modified sol-gel method.

fied sol. As P-25 loading increases, the amount of both rutile and anatase phases increases as is obvious from the main peaks at 2θ angle of 25.4° and 27.5° which are assigned to anatase (1 0 1) and rutile (1 1 0) crystalline phases, respectively. In addition to TiO_2 formed from TTIP precursor, both anatase and rutile phases can also result from P-25 incorporated into sol [16]. Therefore, the increasing amount of both crystal phases with increasing P-25 loading can indicate the enhancement of amounts of P-25 incorporated.

By comparing the XRD spectra of sample prepared via the plain sol-gel (without adding P-25 powder) and samples obtained from PPMSG method, it is suggested that P-25 powder involved in the gel-derived TiO_2 structure favors the rutile formation in the three-dimensional framework, as seen in Fig. 1(b), and therefore it affects the photocatalytic performance of resulting samples. Similar results have been reported by Balasubramanian et al. and Chen et al. [16,17].

Further analysis of XRD revealed that no discernible change in crystal size is noticed for powders synthesized at different P-25 loading, as shown in Fig. 1(b). The size of crystallites in powder derived from the plain sol-gel was 34.2 nm, approximately 8.1 nm smaller that of powders prepared by PPMSG method. Fig. 1(b) also shows the variation of surface area of samples as a function of the P-25 loading. As data show in Fig. 1(b), the surface area of samples slightly increases with increasing the P-25 loading, which confirms a slight change in the crystal size.

FESEM analysis was used to examine the morphology of TiO_2 powder prepared at different loadings of P-25 in the modified sol. Fig. 2 shows the morphology of powders prepared at 0, 10 and 30 g/L P-25 in sol.

As it is obvious by comparing Figs. 2(a) and (b), the grain size of particles formed from the sol containing the P-25 powder is larger than that of particles derived from the plain sol. As suggested by the literature, the P-25 particles may act as sites for nucleation of TiO_2 nanoparticles derived from alkoxide sol [17]. Consequently, the growth of TiO_2 crystallites around the P-25 particles yields the formation of the larger grain size. However, the decrease in average of grain size is also observed with increasing the loading of P-25

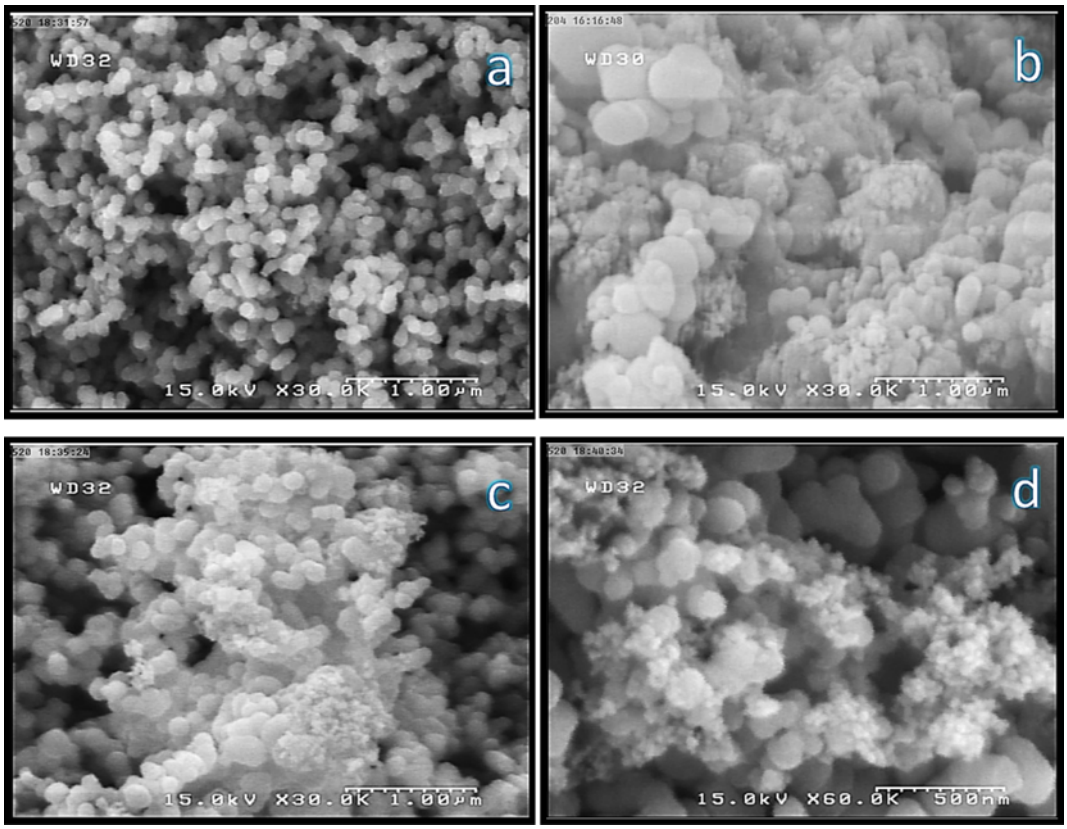

Fig. 2. FESEM images of TiO_2 powders prepared at TTIP concentration: 0.3 M, pH: 1.5 and by the sol containing no P-25 powder (a) 10 g/L P-25 powder (b) and 30 g/L P-25 powder (c) 30 g/L P-25 powder at high magnification (d).

in the modified sol, as it is clear from Figs. 2(b) and (c). The average grain size of powders prepared at various loading of P-25 was measured by measurement software. The average size of grain for the samples obtained at 10, 30 and 50 g/L of P-25 in the modified sol was approximately 185, 141 and 123 nm, respectively. In fact, as P-25 loading increases, the number of crystallites formed from the alkoxide sol is not enough to form a large size grain and the grain size decreases as a result [17].

FESEM analysis of the samples at high magnification shows the formation of sub-grain on the surface of some grains, indicating the secondary nucleation of sol obtained from TiO_2 crystal grains which occurs on the surface of the larger grains formed from the P-25 particles (Fig. 2(d)).

3. Effect of pH

According to some studies, the surface charges of TiO_2 are pH dependent. The adsorption of H^+ or OH^- by TiO_2 particles in sol produces electrical charges on the TiO_2 surface [29]. In acidic or alkaline media (pH<3 or pH>9), a clear and more stable sol can be formed due to the strong repulsive force among the charges particles [29]. In this work, nitric acid was chosen as a sol stabilizer to provide the gelation pH within a range of 1-2.

From XRD analysis presented in Table 3 and Fig. 1(c), TiO_2 powder prepared at higher acidity of pH (i.e., pH=1) exhibits higher degree of crystallinity, indicating large particle size in this sample. It has been reported that isoelectric of TiO_2 powder varies between the pH ranges of 5-6.8 [29]. Bigger TiO_2 particles are formed at pHs away from the range of isoelectric point. Therefore, in this work, higher level of crystalline material was observed for the sample synthesized at higher acidity of medium solution. However, since the surface area and crystallinity degree vary often in different ways [30,31], the decrease in the surface area of samples was noticed with increasing the crystallinity degree (Table 3 and Fig. 1(c)).

Table 3. Physical properties of TiO_2 powders obtained from modified sol-gel method at various pH of gelation, P-25 loading: 30 g/L and TTIP concentration: 0.3 M

Gelation pH value	Crystal size (nm)	Anatase content (%)	S_{BET} (m^2/g)
1	56.71	79	17.31
1.5	42.29	75	22.58
2	31.66	93	28.01

It is also noticed that pH gelation affects the composition of resulting crystal structure. The peak intensity at 2θ=27.51° which is ascribed to rutile (1 1 0) crystalline phase was found to be a trace in sample prepared at pH=2 (Fig. 2 of the supplementary materials). The results show that decreasing acidity in medium solution promotes the anatase formation.

Fig. 3 shows the surface morphology analysis by FESEM for TiO_2 powders prepared via PPMSG method at different gelation pH. As it can be seen, the particle size of sample formed at lower acidity (i.e., pH=2) is smallest compared with two other samples, which is in accordance with the XRD results. As explained above, since lower acidity is closer to the range of isoelectric point, more

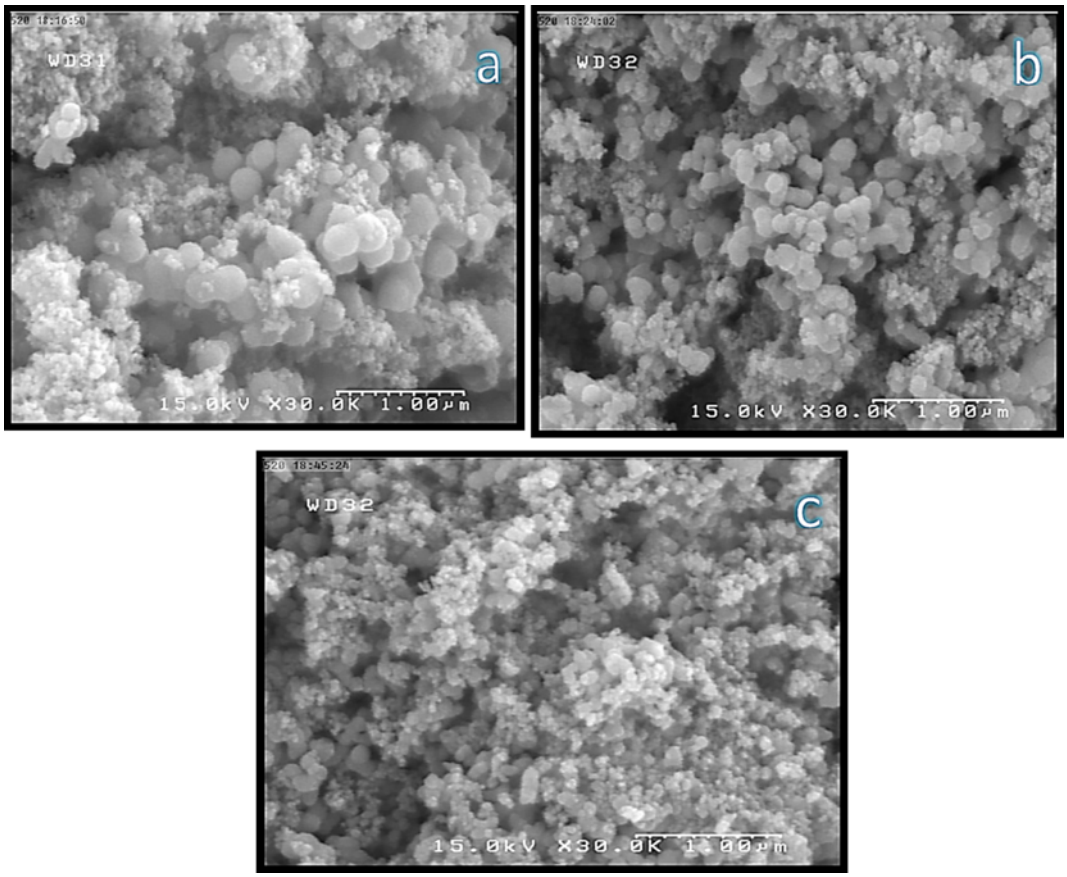

Fig. 3. FESEM images of TiO_2 powders prepared by modified sol-gel method at TTIP concentration: 0.3 M, P-25 loading: 30 g/L and pH: 1 (a) pH: 1.5 (b) and pH: 2 (c).

aggregates and smaller TiO_2 particles are formed. Moreover, powders prepared at 1, 1.5 and 2 of gelation pHs possess average grain size of 198, 134 and 98 nm, respectively. These results confirm the reduction in the grain size of samples with decreasing the acidity in medium solution. Additionally, the presence of sub-grain on the surface of some of the grains can be also noticed, which is ascribed to presence of the P-25 powders in the sol employing like a site for the secondary nucleation of the sol [17].

4. Effect of Physical Properties on Photocatalytic Activity

To show clearly the relationship between the physical properties and the photocatalytic activity, separate graphs are presented based on the available data, as shown in Fig. 4.

As seen in Fig. 4(a), the photocatalytic activity gradually increases with the increase of the crystallite size up to 42.29 nm and decreases at higher value of crystallinity level. The formation of more carrier charge at the surface of photocatalyst with high crystallinity is responsible for the increased photoactivity [32]. The decreased photodegradation can be attributed to the loss of surface area at higher value of crystallite size, since a higher degree of crystallinity is generally achieved through a high-temperature thermal treatment, leading to a decrease in the surface [31].

Fig. 4(b) shows the photocatalytic activity of the samples with different surface area. The degradation percentage of acid dye increases drastically, as the surface area of samples increases. The positive effect of surface area can be ascribed to the increased number of active sites on the surface of catalyst [30]. However, a decrease in acid dye decolorization is observed for the samples with higher surface area. This negative impact can be explained by the fact that powders with a large surface area are usually associated with large amounts of crystalline defects, which accelerates the electron-hole recombination rate leading to a poor photoactivity [33].

By further inspection of data shown in Figs. 4(a) and (b), it can be concluded that the best result of photoactivity is obtained for the samples possessing a high crystallinity level combined with a good surface area, since the surface area and crystallinity degree often vary in opposite ways [30-32].

In addition to the surface area and crystallinity level, the photocatalytic activity can be also affected by the rutile-anatase distribution in the crystalline framework, as shown in Fig. 4(c). The decolorization efficiency increases with increasing the anatase content and decreases as anatase content goes over an optimal value. This behavior can be attributed to the synergistic effect between rutile and anatase [34]. Although, the anatase phase has been proved as more active photocatalyst compared to the rutile phase, the presence of rutile in the TiO_2 crystal structure can influence on the photocatalytic activity [34]. It is assumed that the smaller band gap of rutile (3.02 eV) absorbs the photons and forms the electron-hole pair. Then, the electron transfers from the conductive band of the rutile to electron traps in the anatase phase and the hole can move to the particle surface for reaction [34]. This inhibits the electron-hole recombination improving the photocatalytic performance. However, it should be noted that the anatase/rutile ratio is an important parame-

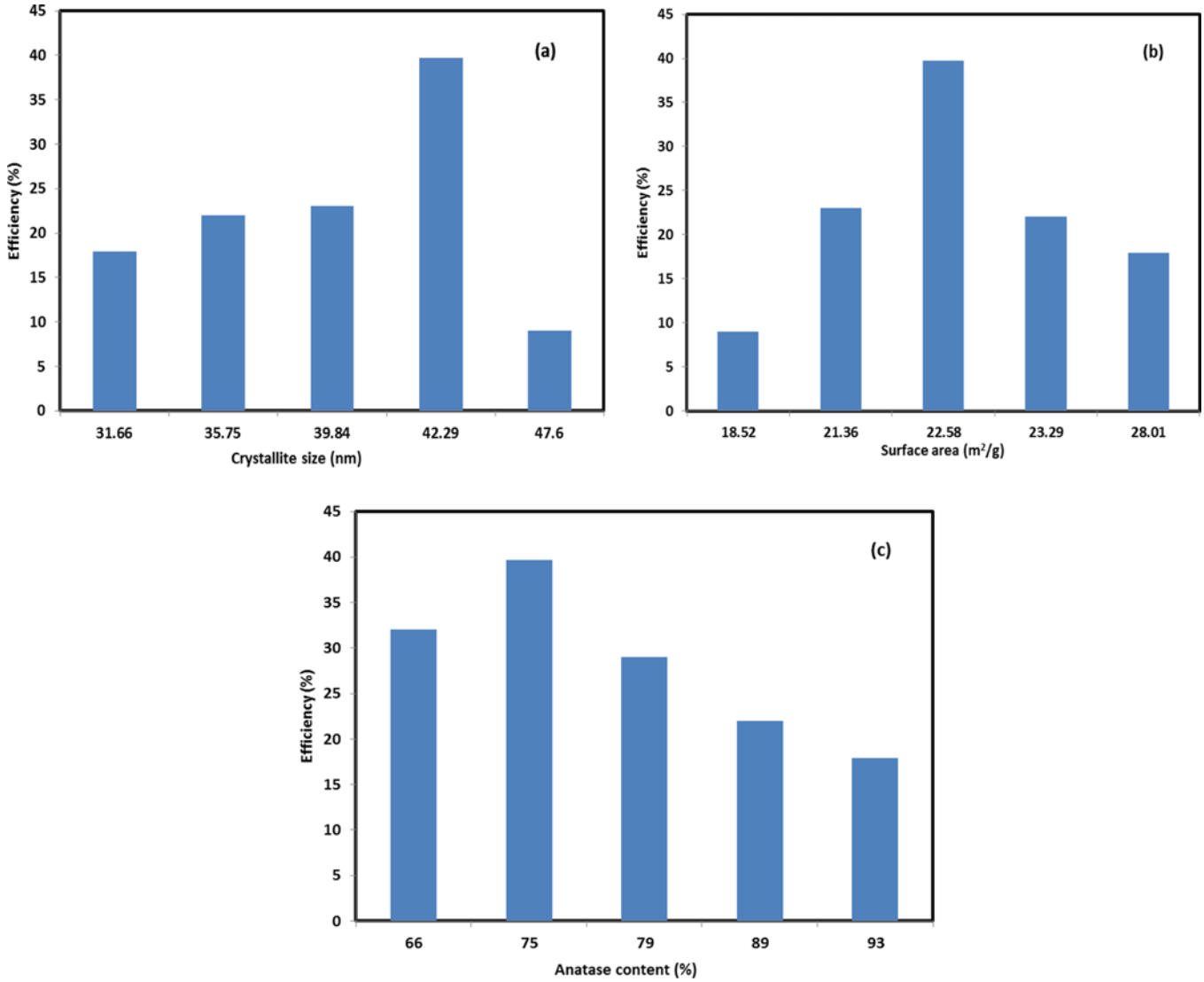

Fig. 4. Variations of photocatalytic activity of TiO_2-P25 for degradation of Acid Red 73 in term of crystallite size (a) surface area (b) anatase content (c).

ter in evaluation of photocatalytic efficiency and there is an optimum value for the rutile content [30]. As shown in Fig. 4(c), the best photocatalytic activity is observed for the sample that contains the crystalline composition of rutile and anatase close to that of commercial P-25 TiO_2 (70/80 : 30/20). A similar result has been reported by [30].

5. Mathematical Modeling and Optimization of Factors

5-1. Model Fitting and Analysis of Variance (ANOVA)

The experimental results obtained from the design matrix and the predicted responses based on the experimental design proposed by CCD are presented in Table 1 of the supplementary materials.

Depending upon the presented experimental design, the relationship between the response and the studied variables was derived and expressed by the following empirical second-order polynomial equation in actual form:

$$\%\ \text{degradation} = -170.00171 + 4.26293 \times TTIP + 4.28598 \times P25 + 150.95228 \times pH - 0.04118 \times TTIP \times P25 + 0.79902 \times TTIP \times pH - 0.32880 \times P25 \times pH - 0.14758 \times TTIP^2 - 0.041896 \times P25^2 - 55.24231 \times pH^2$$

The results obtained from the analysis of variance (ANOVA) at 95% confidence level are given in Table 2 of the supplementary materials.

According to the ANOVA results (Table 4), the model F-value of

Table 4. ANOVA results for the response surface quadratic model

Source	Sum of squares	Degree of freedom	Mean squares	F value	P value
Model	2190.23	9	243.36	45.75	<0.0001
Residual	53.19	10	5.32		
Lack of fit	38.47	5	7.69	2.61	0.1578
Pure error	14.73	5	2.95		
Total	2243.43	19			
Std. Dev.	2.31				

45.75 implies the model is significant. There is only a 0.01% chance that the model F value could occur due to noise. The p value for the model, which is less than 0.0001, also indicates that the model is significant. The lack-of-fit F-value of 2.61 implies that the lack of fit is not significant relative to the pure error. There is a 15.78% chance that the lack-of-fit F-value could occur due to noise. The non-significant lack-of-fit term indicates the ability of the model to predict the experimental results accurately.

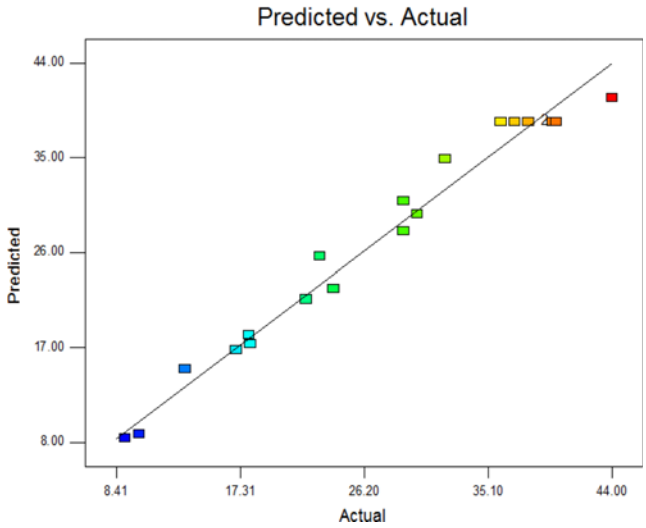

Fig. 5. Experimental values plotted against the predicted values derived from the model.

The good predictability of the model was also confirmed by the Pred R-Squared of 0.8566, which is in reasonable agreement with the Adj R-Squared of 0.9549. Fig. 5 displays the predicted values of responses versus the observed ones, confirming the accuracy of model for prediction of the degradation efficiency of Acid Red 73.

The p-values were applied as a tool to evaluate the importance of each factor. Among the studied variables, the P-25 loading (x_2), pH gelation (x_3) and the second-order effect of factors (x_{ii}^2) are highly significant parameters with $p<0.001$. Based on the negative coefficients of quadratic terms x_{ii}^2 in the polynomial expression, an excess of TTIP concentration (x_1), the P-25 loading (x_2) and pH gelation (x_3) in the system produces a negative influence on the photocatalytic performance (decreased Acid Red 73%degradation) [23,35]. Moreover, the interaction effect between the concentration of TTIP (x_1) and P-25 loading (x_2) is significant at $p<0.05$. The negative coefficient of x_1x_2 parameter in the polynomial expression indicates an antagonistic effect between these variables [23,35]. Furthermore, the p value >0.05 means that the model term is insignificant. Table 2 of the supplementary materials shows that the first-order effect of TTIP concentration (x_1) and the interactions between TTIP concentration and pH gelation and between P-25 loading and pH gelation are insignificant.

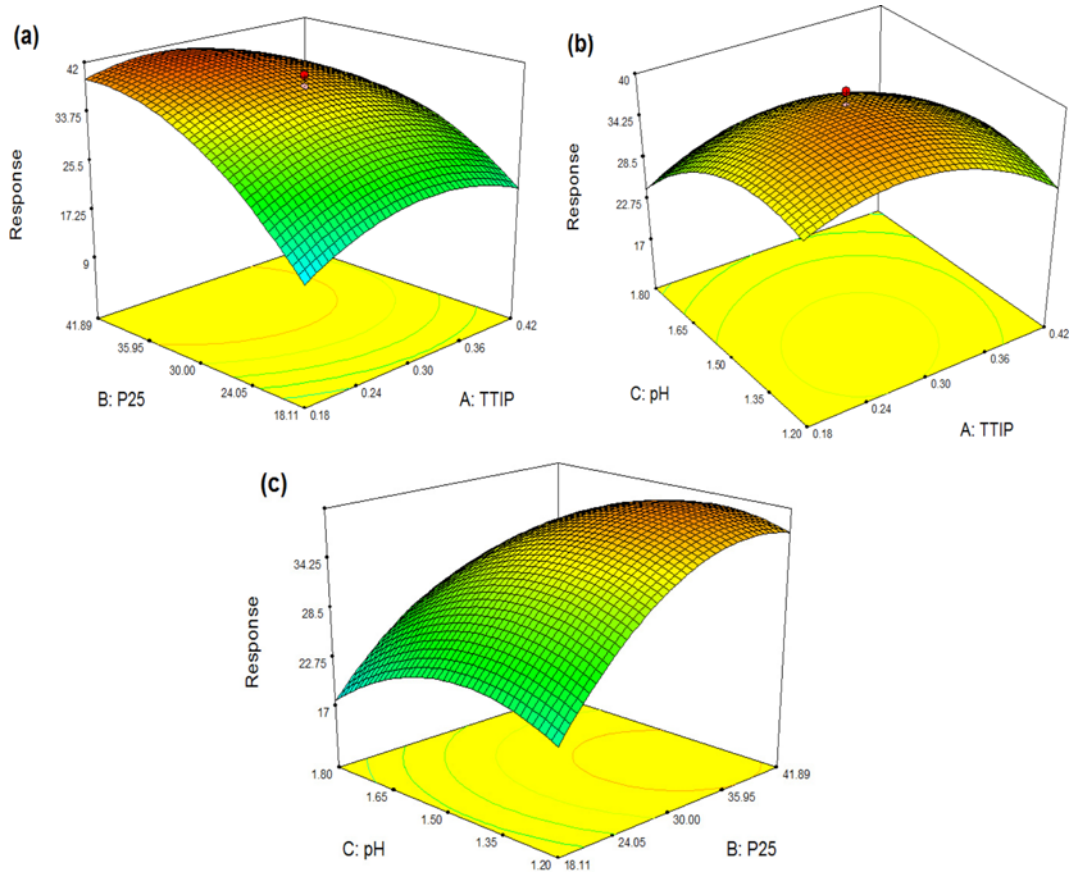

Fig. 6. Effects of TTIP concentration and P-25 loading on Acid Red 73 degradation (Gelation pH: 1.5) (a) Effects of TTIP concentration and gelation pH on Acid Red 73 degradation (P-25 loading: 30 g/L) (b) Effects of P-25 loading and gelation pH on Acid Red 73 degradation (TTIP concentration: 0.3 M) (c).

According to the monomial coefficient values of the regression model, $p(x_1)=0.0835$ (TTIP concentration), $p(x_2)<0.0001$ (P-25 loading) and $p(x_3)=0.0001$ (pH gelation), the order of importance among the factors is P-25 loading (x_2)>pH gelation (x_3)>TTIP concentration (x_1). The resultant ranking can be also attributed to the experimental range of independent variables considered in this study.

5-2. Response Surface Analysis

The model-predicted response can be displayed graphically in three-dimensional plots to provide a clearer view of the response surface and a better understanding of interactions between variables within the range considered [28]. This effective tool is also widely used to find the optimal value of parameters [28]. The results of the interactions between three independent variables and decolorization efficiency are shown in Fig. 6.

Fig. 6(a) shows the simultaneous effect of TTIP concentration and P-25 loading on Acid Red 73 degradation. Degradation increases with an increase in TTIP from 0.1 to 0.28 M and decreases gradually when the TTIP concentration increases beyond 0.3 M. This behavior can be attributed to the rutile-anatase distribution in the crystalline framework, as shown in Fig. 1(a). Based on the XRD analysis, the rutile content in TiO_2 catalysts increases with increasing TTIP amount to a middle concentration and decreases as TTIP concentration goes over an optimal value. Although the anatase phase of TiO_2 has been reported to be more active as a photocatalyst compared with the rutile, the synergistic effect between rutile and anatase can improve the photocatalytic performance of TiO_2 [34], as described earlier in section 3.4.

However, the high loading of P-25 slows down the positive effect of TTIP concentration significantly and accelerates its negative effect on the photocatalytic performance. Incorporating P-25 loading into the sol favors the rutile formation in resulting crystal structure, as XRD results have shown. Therefore, the rutile content of catalyst increases at high loading of P-25. Although the presence of rutile in the crystalline structure improves the photocatalytic activity, the anatase/rutile proportion can be also an important parameter in evaluation of photocatalytic efficiency. As mentioned in section 3.4, the best result of photoactivity is observed for the sample possesses the crystalline composition of rutile and anatase close to that of commercial P-25 TiO_2 (70/80 : 30/20) [30]. Generally, both P-25 loading above 35 g/L and TTIP concentration more than 0.3 M decrease the decolorization of catalyst efficiency. This trend leads to the conclusion that the interaction effects of TTIP concentration and P-25 loading beyond the optimum value do not enhance the decolorization efficiency of Acid Red 73.

The effects of TTIP concentration and pH gelation on Acid Red 73 degradation efficiency are shown in Fig. 6(b). The effect of TTIP concentration on the color removal efficiency exhibited similar trends. As explained above, TTIP concentration in the gel-derived titania affects the crystalline composition of rutile and anatase and consequently induces the variation of catalyst efficiency. At higher value of gelation pH, the increased rutile content and the decreased size of particles can slightly enhance the negative impact of TTIP concentration. Powders with a small size of particles are usually associated with large amounts of crystalline defects, which favors the electron-hole recombination leading to a poor photoactivity [33]. However, it is also noted that small grain size can confer sufficiently active surface to adsorb organic molecules and promotes photocatalytic efficiency, as a result. Therefore, as shown in Fig. 6(b), there is an optimum value for gelation pH leading to an optimal value for particles size and consequently high level of crystallinity combined with good surface area, which contributes to high efficiency of TiO_2 catalysts.

Fig. 6(c) shows the effects of P-25 loading and gelation pH on decolorization. The influence of loading of P-25 on the degradation of Acid Red 73 is highly significant. As the amount of P-25 powder incorporated into sol increases, the degradation percentage of acid dye increases drastically, whether gelation pH has a low or high value. This positive effect can be ascribed to the increased rutile content in the final crystal structure, which confers more electron capture traps. However, at higher loading of P-25, a slight decrease in acid dye decolorization is observed. This negative impact can be explained by decreasing the grain size of samples at higher loading of P-25, as SEM analysis shown. As explained, small grain size of catalyst may imply poor crystallinity, which induces high concentration of defects and each one acts as a recombination center [30].

5-3. Optimization of the Synthesis Conditions

The optimal conditions for the degradation of Acid Red 73 were determined on the basis of the desirability function. In fact, the desirability function is an objective function that ranges from zero outside of the limits to one at the goal. The numerical optimization program was applied to find a set of conditions that maximizes this function. Five possible goals exist as desirability indices: none, maximum, minimum, target and within range. A minimum and a maximum level must be provided for each parameter included in the optimization. A weight or importance can be assigned to a goal, indicating the significance degree of the upper/lower bounds or the target value. For such studies, the maximum degradation, which is the main objective of optimization, was considered by adjusting the 'importance' to 5 like in the previous work [28]. The criteria for all factors in correspondence with degradation percentage are given in Table 5.

Based on the settings and boundaries described above, the optimal synthesis conditions for maximum Acid Red 73 degradation efficiency (42.88%) were found to be a TTIP concentration of 0.25 M, P-25 loading of 39.76 g/L and a gelation pH value of 1.34.

5-4. Model Validation and Confirmation

Verification experiments were carried out at the optimal synthe-

Table 5. Optimization of the individual responses (di) to find the overall desirability response (D)

Name	Goal	Lower limit	Upper limit	Lower weight	Upper weight	Importance
TTIP concentration	In the range	0.1	0.5	1	1	3
P-25 loading	In the range	10	50	1	1	3
Gelation pH	In the range	1	2	1	1	3
Response (degradation %)	Maximize	9	44	1	1	5

sis conditions obtained from the experimental design proposed by CCD to confirm the adequacy of the model for predicting of the maximum percentage degradation of Acid Red 73. An average degradation of 43.03% was derived from three replicative experiments performed by titania synthesized under optimal conditions. The standard deviation of three replicative runs was also determined relative to average of degradation (43.03%) as the following equation:

$$\text{Std. Dev} = \sqrt{\frac{\sum_{i=1}^{n}(x_i - \bar{x})^2}{n-1}}$$

where x_i is the observed Acid Red 73 degradation percentage in each replicative experiment (42.95%, 43% and 43.20%), $\bar{x}$ is the mean value of degradation percentage (43.03%), and n is the number of experiments, which was 3 in this case.

Moreover, the relative error was also determined for three replicative experiments. The error was calculated relative to average maximum degradation, as follows:

$$\text{Relative error} = \frac{|x_i - \bar{x}|}{x_i}$$

Based on the observed Acid Red 73 degradation percentage in each replicative experiment (42.95%, 43% and 43.20%), the error in each run relative to average maximum degradation (42.03%) was found to be 0.23, 0.11 and 0.34, respectively. In addition, the average error from the values of relative errors was also calculated. The average error of 0.22 and standard deviation of 0.169 imply that there is good agreement between the experimental and predicted results, confirming the validity of the model for simulating the photodegradation of Acid Red 73.

6. Evaluation of TiO_2 Film Coated Alumina Foams

At the optimal experimental conditions derived by response surface methodology, the titania nanoparticles were coated on reticulated alumina foam using sol precipitated by modified sol-gel method and typical sol-gel procedure (without adding P-25 powder). The structural properties of the immobilized photocatalyst were characterized by XRD and SEM analysis.

The surface area of the alumina foams before and after coating with the film made by modified sol-gel technique exhibit the values of 0.2 and 7.26 m^2/g, respectively. These values indicate that good photocatalytic efficiency can be expected from the coated samples.

Table 6. Physical properties of TiO_2 powder and films obtained from modified sol-gel method and the typical sol-gel method at optimal conditions derived from experimental design

Method	Crystal size (nm)	Anatase content (%)
Powders prepared by PPMSG method	43.06	78
Film prepared by PPMSG method	46.3	82
Film prepared by sol-gel method	39.2	91

The XRD patterns of plain TiO_2 powder prepared by PPMSG method and immobilized titania nanoparticles on alumina foams are shown in Fig. 3 of the supplementary materials. Despite the peak observed at 2θ=66.53°, which is ascribed to alumina, almost no significant change in the crystal structure of the as-prepared samples can be noted due to immobilization process. Furthermore, the size of the crystallites calculated using Scherrer's equation and the anatse content of the coated samples have been summarized in Table 6. The results show that the size of anatase crystallites of the as-prepared products, which was served as a measure of TiO_2 crytsallinity, is practically the same and no significant variation of crystal size is observed due to the presence of P-25 powder and the immobilization process. However, by inspection of Table 6, it is noticed that the incorporation of P-25 powder into film promotes formation of the rutile component in the crystal structure, which can influence the photocatalytic activity of catalyst.

SEM photographs of the TiO_2 films prepared by modified sol-gel and plain sol-gel (without P-25 in the sol) are shown in Fig. 7. SEM micrograph of alumina foam coated with modified titania films indicates the presence of microcracks in the film. The formation of microcracks can be attributed to the P-25 powder incorporated into the sol. Since P-25 powder has relatively large density and low porosity, its loading in the sol during the synthesis procedure leads to the formation TiO_2 gels with decreased permeability. As reported by the literature, the decreased permeability of the gels prepared with the PPMSG method is one of the important factors that results in the formation of microcracks in the films [17]. It is believed that the presence of microcracks in the film is beneficial to the exposure of titania nanoparticles within the inner layers to the solution and can

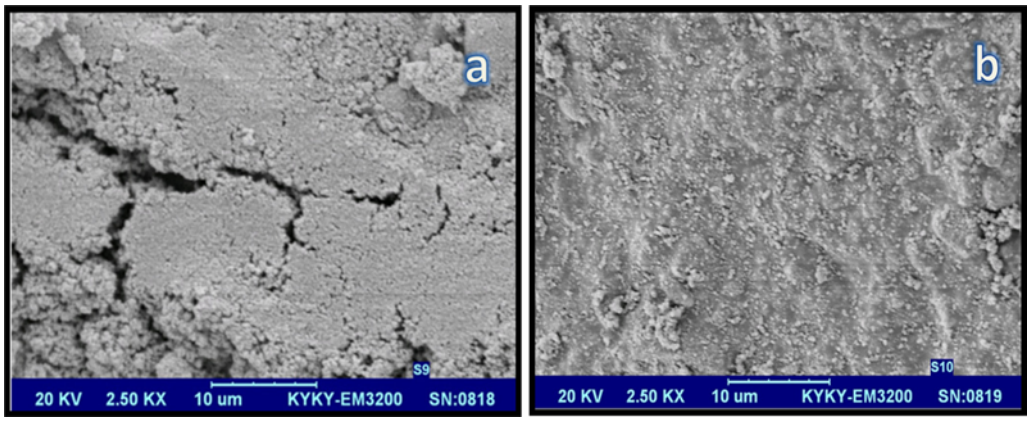

Fig. 7. SEM images of the surface of TiO_2 films made from the precursor sol prepared at optimal conditions with P-25 powder (a) without P-25 powder (b).

improve the photocatalytic efficiency of the as-prepared films.

Since for a large application, the durability of the film is a very important parameter [17], the stability of TiO_2 film immobilized on the alumina foam was investigated for three types of film prepared by three different methods: 1) suspension of commercial TiO_2 (P-25) 2) sol synthesized by a typical sol-gel procedure 3) TiO_2 sol made by PPMSG method. To provide a slurry of P-25 powder in the first method, a solution of P-25 powder with concentration obtained from optimization was prepared (39.76 g/L). However, after the coating procedure, the calcination process was carried out at 600 °C for 1 h with a heating and cooling rate of 1 °C/min. The preparation procedure in detail has been reported in our previous works [21,28]. Both sols used in plain sol-gel and modified sol-gel were prepared at optimal conditions derived from the experimental design. It is clear that sol synthesized in unmodified sol-gel was made without adding P-25. The initial dye concentration and volume of solution used in this experiment were 20 mg/L and 250 mL, respectively. TiO_2 films were immobilized on the substrate with three time of coating using each TiO_2 solution obtained as the above, and the change of TiO_2 weight immobilized on the alumina foam was investigated after 2 h in the reactor under UV irradiation, where the stability was studied as the difference of TiO_2 weight immobilized on the foams before and after the photodegradation process, as suggested by [10].

As shown in Fig. 8, TiO_2 nanoparticles synthesized by PPMSG method and immobilized on the alumina foam exhibit best stability among three types, where 88 wt% of the initial weight remained. It indicates the bond force between the TiO_2 particles and alumina surface was high, even though TiO_2 film was cracked. This result shows good adhesion of film prepared in the modified sol to the support and demonstrates good stability and durability of films obtained from modified sol-gel for applications in water treatment.

To evaluate the photocatalytic activity of the immobilized TiO_2 particles on alumina foams, five decolorization processes were compared for Acid Red 73 (dye: 20 mg/L, pH: 6 and H_2O_2: 0.55 mg/L): alumina foam with UV irradiation (a), the foam coated with the film made by modified sol-gel technique without UV irradiation (b), immobilized TiO_2 formed from slurries of commercial TiO_2 (P-25) with UV irradiation (c), coated sample prepared using TiO_2 sol synthesized by a typical sol-gel procedure with UV irradiation (d), and TiO_2-coated alumina derived from TiO_2 sol made by PPMSG method with UV irradiation (e). It is pointed that for the preparation of the film in process (e), a slurry of P-25 powder was prepared and then the alumina foam was dipped into the as-prepared slurry for coating the film on the foam. The loading of P-25 in this solution (39.76 g/L) was the optimal value obtained from optimization. However, after the coating procedure, the calcination process was carried out as earlier implied. It is also noted that both sols used in plain sol-gel and modified sol-gel were prepared at optimal conditions derived from the experimental design.

Experimental results show that the adsorption of Acid Red 73 on reticulated alumina foam becomes saturated after 60 min under UV light radiation, since the dye concentration does not change further with prolonged UV. This indicates that alumina foam does not possess any photocatalytic activity (curve (a) in Fig. 9), and the variation of dye concentration in this period can be attributed to the presence of UV-H_2O_2. The ceramic alumina foams coated with the film prepared by PPMSG procedure show a higher catalytic activity in the absence of UV radiation, since the saturated adsorption capacity is higher in comparison with the uncoated alumina foams (curve (b) in Fig. 9). The deposition of TiO_2 nanoparticles on the foam may lead to the affinity of the alumina for acid dye. It can be also attributed to the increased surface area of the support after coating. By comparison of the acid dye removal with and without UV radiation (curves (b), (c), (d) and (e) in Fig. 9), it can be concluded that photocatalytic degradation is predominant in the disappearance of Acid Red 73 and the adsorption is insignificant.

According to the data shown in Fig. 9 (curves (d) and (e)), the photocatalytic activity of films formed from sols containing P-25 powder is higher than that of films made by typical sol-gel technique. The microcrack formation in the films prepared from modified sol-gel can be responsible for the higher catalytic activity of the alumina coated with the as-prepared films. The presence of microcracks may have a positive effect on the photocatalytic performance of the film regarding UV light penetration and availability of organic contaminates to TiO_2 particles which may be in the inner layers. In addition, the presence of P-25 powder in the resultant catalyst can

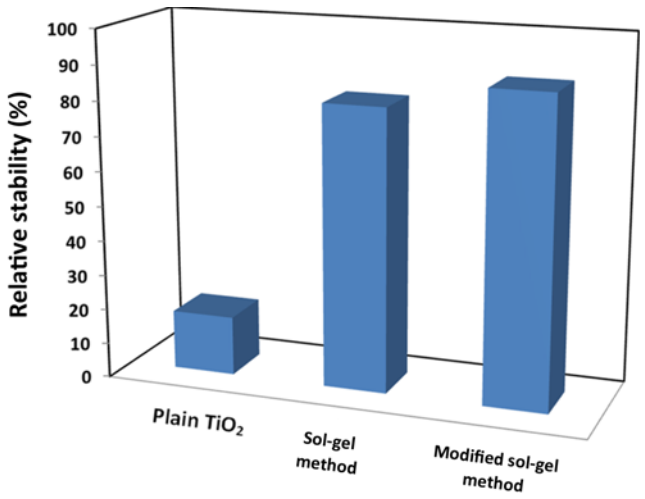

Fig. 8. Stability of film immobilized on the alumina foam for three methods: P-25, sol-gel method, and modified sol-gel method.

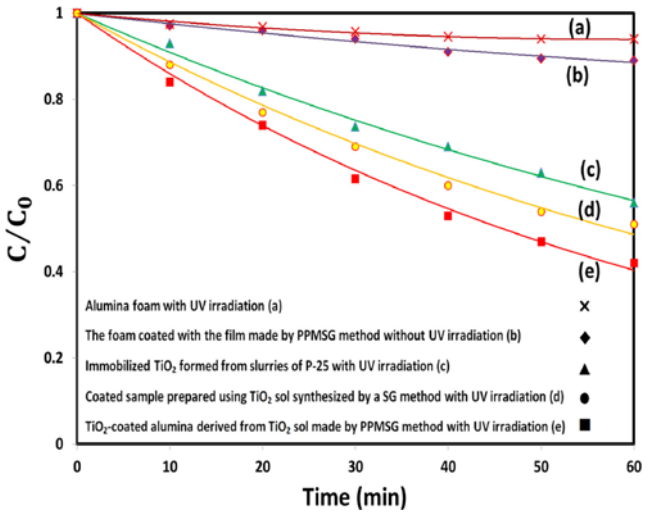

Fig. 9. Effect of photocatalyst on the degradation of Acid Red 73.

increase the interface area between the TiO_2 catalyst and liquid, and consequently improve the photocatalytic efficiency. Moreover, the films formed from the sol prepared via the modified sol-gel technique show higher activity than that made from the suspension of commercial TiO_2 (P-25), as shown in Fig. 9 (curves (c) and (e)). It is assumed that this difference can be caused by the difference in adhesion of TiO_2 film immobilized on the alumina foam. As the results show, better stability and durability is offered by the films obtained from the sol synthesized by the modified sol-gel method compared to that prapared by the slurries of P-25 powders.

CONCLUSION

The effects of TTIP concentration, P-25 loading and gelation pH on the structural properties of TiO_2 synthesized by a modified sol-gel method were investigated. Based on XRD analysis SEM results and BET technique, the crystalline composition of rutile and anatase was found to be affected by these parameters, whereas P-25 loading and gelation pH indicated an additional effect on the level of crystallinity, the particle size and the surface area of the as-prepared TiO_2 catalysts.

Subsequently, the experimental design methodology was used to optimize the selected parameters for synthesize of TiO_2 nanoparticles using the modified sol-gel method for the degradation of Acid Red 73. Under the optimized conditions of a 0.25 M TTIP concentration, 39.76 g/L P-25 loading and a pH value of 1.34, the degradation efficiency of Acid Red 73 approached 42.88% after 1 h. Regression analysis with an R^2 value of 0.9549 showed a good agreement between the experimental results and the predicted value.

At the optimal experimental conditions, the titania nanoparticles were immobilized on reticulated alumina foam using sol precipitated by modified sol-gel method. Compared with the films prepared by the sol-gel method and those made from the slurries of P-25 powder, the films synthesized by modified sol-gel route exhibit higher photocatalytic activity. At the same time, better stability and adhesion of the as-prepared film coated on alumina foam leads to consider it as an effective alternative for large-scale applications of water treatment.

SUPPORTING INFORMATION

Additional information as noted in the text. This information is available via the Internet at http://www.springer.com/chemistry/journal/11814.

REFERENCES

1. D. F. M. Oliveira, P. S. Batista, P. S. Muller Jr., V. Velani, M. D. França, D. R. de Souza and A. E. H. Machado, *Dyes Pigm.*, **92**, 563 (2012).
2. T. Ochiai, K. Nakata, T. Murakami, A. Fujishima, Y. Yao, D. A. Tryk and Y. Kubota, *Water Res.*, **44**, 904 (2010).
3. D. Wang, L. Xiao, Q. Luo, X. Li, J. An and Y. Duan, *J. Hazard. Mater.*, **192**, 150 (2011).
4. R. Thiruvenkatachari, S. Vigneswaran and I. Moon, *Korean J. Chem. Eng.*, **25**, 64 (2008).
5. M. N. Chong, B. Jin, C. W. K. Chow and C. Saint, *Water Res.*, **44**, 2997 (2010).
6. A. Y. Shan, T. I. M. Ghazi and S. A. Rashid, *Appl. Catal. A: Gen.*, **389**, 1 (2010).
7. G. Plesch, M. Gorbár, U. F. Vogt, K. Jesenák and M. Vargová, *Mater. Lett.*, **63**, 461 (2009).
8. M. Vargová, G. Plesch, U. F. Vogt, M. Zahoran, M. Gorbár and K. Jesenák, *Appl. Surf. Sci.*, **257**, 4678 (2011).
9. I. J. Ochuma, O. O. Osibo, R. P. Fishwick, S. Pollington, A. Wagland, J. Wood and J. M. Winterbottom, *Catal. Today*, **128**, 100 (2007).
10. C. S. Ryu, M.-S. Kim and B.-W. Kim, *Chemosphere*, **53**, 765 (2003).
11. U. G. Akpan and B. H. Hameed, *Appl. Catal. A: Gen.*, **375**, 1 (2010).
12. C.-J. Tseng, C.-H. Wang and K.-W. Cheng, *Sol. Energy Mater. Sol. C.*, **96**, 33 (2012).
13. M. A. Behnajady, H. Eskandarloo, N. Modirshahla and M. Shokri, *Desalination*, **278**, 10 (2011).
14. M. Bestetti, D. Sacco, M. F. Brunella, S. Franz, R. Amadelli and L. Samiolo, *Mater. Chem. Phys.*, **124**, 1225 (2010).
15. Y. Zhu, L. Zhang, L. Wang, Y. Fu and L. Cao, *J. Mater. Chem.*, **11**, 1864 (2001).
16. G. Balasubramanian, D. D. Dionysiou, M. T. Suidan, V. Subramanian, I. Baudin and J. M. Laîné, *J. Mater. Sci.*, **38**, 823 (2003).
17. Y. Chen and D. D. Dionysiou, *Appl. Catal. B: Environ.*, **62**, 255 (2006).
18. A. Fernández, G. Lassaletta, V. M. Jiménez, A. Justo, A. R. González-Elipe, J. M. Herrmann, H. Tahiri and Y. Ait-Ichou, *Appl. Catal. B: Environ.*, **7**, 49 (1995).
19. M. Keshmiri, M. Mohseni and T. Troczynski, *Appl. Catal. B: Environ.*, **53**, 209 (2004).
20. S.-M. Lam, J.-C. Sin and A. Mohamed, *Korean J. Chem. Eng.*, **27**, 1109 (2010).
21. M. Vaez, A. Z. Moghaddam, N. M. Mahmoodi and S. Alijani, *Process. Saf. Environ.*, **90**, 56 (2012).
22. S. N. Hosseini, S. M. Borghei, M. Vossoughi and N. Taghavinia, *Appl. Catal. B: Environ.*, **74**, 53 (2007).
23. V. A. Sakkas, P. Calza, M. A. Islam, C. Medana, C. Baiocchi, K. Panagiotou and T. Albanis, *Appl. Catal. B: Environ.*, **90**, 526 (2009).
24. V. A. Sakkas, M. A. Islam, C. Stalikas and T. A. Albanis, *J. Hazard. Mater.*, **175**, 33 (2010).
25. H.-L. Liu and Y.-R. Chiou, *Chem. Eng. J.*, **112**, 173 (2005).
26. M. N. Chong, H. Y. Zhu and B. Jin, *Chem. Eng. J.*, **156**, 278 (2010).
27. S. Royaee, M. Sohrabi and N. Fallah, *Korean J. Chem. Eng.*, **29**, 1577 (2012).
28. M. Vaez, A. Zarringhalam Moghaddam and S. Alijani, *Ind. Eng. Chem. Res.*, **51**, 4199 (2012).
29. C. Su, B. Y. Hong and C. M. Tseng, *Catal. Today*, **96**, 119 (2004).
30. Y. Bessekhouad, D. Robert and J. V. Weber, *J. Photochem. Photobiol. A. Chem.*, **157**, 47 (2003).
31. S. Ahmed, M. G. Rasul, W. N. Martens, R. Brown and M. A. Hashib, *Desalination*, **261**, 3 (2010).
32. A. R. Khataee and M. B. Kasiri, *J. Mol. Catal. A. Chem.*, **328**, 8 (2010).
33. O. Carp, C. L. Huisman and A. Reller, *Prog. Solid State Chem.*, **32**, 33 (2004).
34. S. Ahmed, M. G. Rasul, R. Brown and M. A. Hashib, *J. Environ. Manage.*, **92**, 311 (2011).
35. D. Vildozo, C. Ferronato, M. Sleiman and J. M. Chovelon, *Appl. Catal. B: Environ.*, **94**, 303 (2010).

Supporting Information

Characterization of TiO_2-coated ceramic foam prepared by modified sol-gel method and optimization of synthesis parameters in photodegradation of Acid Red 73

Somayeh Alijani, Abdolsamad Zarringhalam Moghaddam†, Mohammad Vaez, and Jafar Towfighi

Department of Chemical Engineering, Tarbiat Modares University, Jalal Ale Ahmad Highway,
P. O. Box 14155-143, Tehran, Iran
(*Received 9 December 2012 • accepted 10 July 2013*)

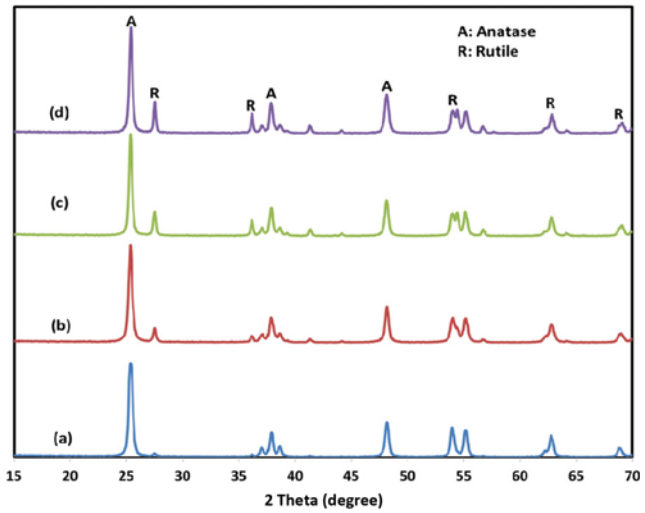

Fig. 1. XRD patterns of TiO_2 powders prepared with TTIP concentration: 0.3 M, pH: 1.5 and the sol containing no P-25 powder (a) 10 g/L P-25 powder (b) 30 g/L P-25 powder (c) and 50 g/L P-25 powder (d).

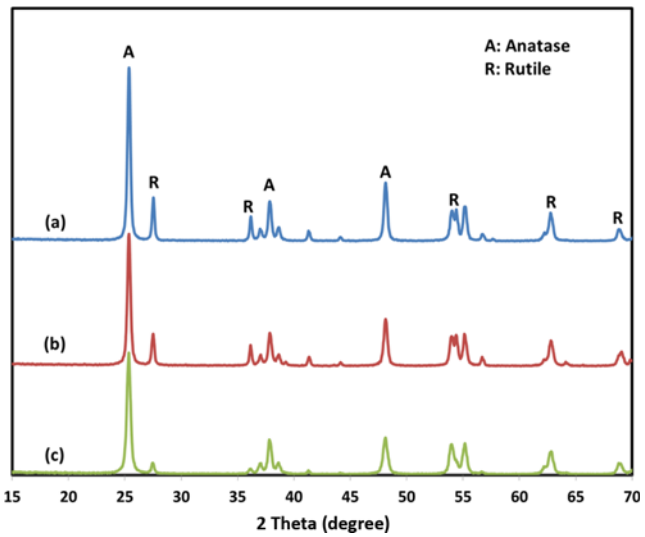

Fig. 2. XRD patterns of TiO_2 powders prepared by modified sol-gel method at TTIP concentration: 0.3 M, P-25 loading: 30 g/L and pH: 1 (a) pH: 1.5 (b) and pH: 2 (c).

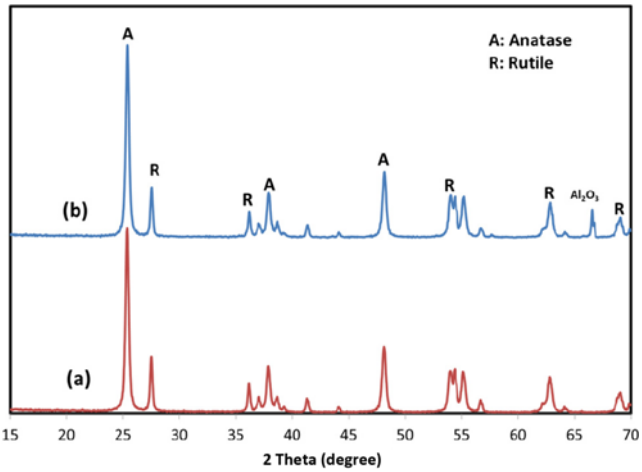

Fig. 3. XRD patterns of TiO_2 powders (a) Immobilized titania nanoparticles coated on the alumina (b) both prepared by modified sol-gel method at optimal conditions.

Table 1. Experimental designs and experimental results with predicted values

Run	Expereimental conditions			Acid Red 73 degradation (%)	
	x_1	x_2	x_3	Experimental	Predicative
1	0.42	18.11	1.80	13.3	15.03
2	0.10	30.00	1.50	23	25.65
3	0.30	30.00	1.50	40	38.39
4	0.42	41.89	1.80	24	22.60
5	0.18	18.11	1.20	17	18.25
6	0.50	30.00	1.50	22	21.61
7	0.30	30.00	1.50	38	38.39
8	0.30	30.00	1.50	39.72	38.39
9	0.30	30.00	1.50	36	38.39
10	0.18	18.11	1.80	10	8.78
11	0.30	30.00	1.50	37	38.39
12	0.18	41.89	1.80	29	28.00
13	0.30	30.00	1.00	29	30.90
14	0.42	41.89	1.20	30	29.63
15	0.30	50.00	1.50	32	34.85
16	0.30	30.00	1.50	40	38.39
17	0.42	18.11	1.20	18	17.40
18	0.18	41.89	1.20	44	40.67
19	0.30	30.00	2.00	17.9	18.25
20	0.30	10.00	1.50	9	8.41

Table 2. Coefficients of regression and their significances

Factor	Coefficient estimate	Degree of freedom	Standard error	F-value	95% Confidence interval low	95% Confidence interval High	P-value
Intercept	38.39	1	0.94	-	36.29	40.48	-
x_1	−1.20	1	0.62	3.69	−2.59	0.19	0.0835
x_2	7.86	1	0.62	158.72	6.47	9.25	<0.0001
x_3	−3.76	1	0.62	36.33	−5.15	−2.37	0.0001
$x_1 x_2$	−2.91	1	0.82	12.76	−4.73	−1.10	0.0051
$x_1 x_3$	1.41	1	0.82	3.00	−0.40	3.23	0.1139
$x_2 x_3$	−1.16	1	0.82	2.03	−2.98	0.65	0.1844
x_1^2	−5.22	1	0.61	73.76	−6.57	−3.86	<0.0001
x^2_2	−5.93	1	0.61	95.11	−7.28	−4.57	<0.0001
x^2_3	−4.88	1	0.61	64.59	−6.24	−3.53	<0.0001